NeuroImage 60 (2012) 370–375

Contents lists available at SciVerse ScienceDirect

NeuroImage

journal homepage: www.elsevier.com/locate/ynimg

# Cortico-subthalamic white matter tract strength predicts interindividual efficacy in stopping a motor response

Birte U. Forstmann [a,*], Max C. Keuken [a,b], Sara Jahfari [a], Pierre-Louis Bazin [b], Jane Neumann [b,c], Andreas Schäfer [b], Alfred Anwander [b], Robert Turner [b]

[a] Cognitive Science Center Amsterdam, University of Amsterdam, Amsterdam, Netherlands
[b] Max Planck Institute for Human Cognitive and Brain Sciences, Leipzig, Germany
[c] Leipzig University Medical Center, IFB Adiposity Diseases, Leipzig, Germany

ARTICLE INFO

*Article history:*
Received 31 August 2011
Revised 8 November 2011
Accepted 15 December 2011
Available online 28 December 2011

*Keywords:*
Subthalamic nucleus
7T magnetic resonance imaging
Atlas
Diffusion weighted imaging
Stop-signal paradigm

ABSTRACT

The subthalamic nucleus (STN) is a small but vitally important structure in the basal ganglia. Because of its small volume, and its localization in the basal ganglia, the STN can best be visualized using ultra-high resolution 7 Tesla (T) magnetic resonance imaging (MRI). In the present study, first we individually segmented 7T MRI STN masks to generate atlas probability maps. Secondly, the individually segmented STN masks and the probability maps were used to derive cortico-subthalamic white matter tract strength. Tract strength measures were then taken to test two functional STN hypotheses which account for the efficiency in stopping a motor response: the right inferior fronto-subthalamic (rIFC-STN) hypothesis and the posterior medial frontal cortex-subthalamic (pMFC-STN) hypothesis. Results of two independent experiments show that increased white matter tract strength between the pMFC and STN results in better stopping behaviour.



## Introduction

Central for successful everyday life is the ability to control our actions by overcoming unwanted response tendencies or terminating ongoing movements. It is widely recognized that the cortico-basal ganglia network controls motor performance (Bogacz et al., 2010; Mink, 1996; Nambu et al., 2002). More specifically, within this network, the subthalamic nucleus (STN) is hypothesized to receive excitatory cortical input which in turn leads to a slowing or termination of movements. However, up to now it remains elusive which cortical region in concert with the STN implements the stopping of a motor response. Two hypotheses were formulated: the right inferior fronto-subthalamic (rIFC-STN) hypothesis and the posterior medial frontal cortex-subthalamic (pMFC-STN) hypothesis (Aron and Poldrack, 2006; Aron et al., 2007; Bogacz et al., 2010; Frank et al., 2007b). Both hypotheses posit that an emphasis on accuracy promotes excitatory input from cortex, i.e., areas in pMFC such as right inferior frontal cortex (rIFC) or anterior cingulate cortex (ACC)/pre-supplementary motor cortex (pre-SMA) to the STN. In turn, increased STN activity may lead to slower responses or even a complete interruption of planned motor responses (Frank et al., 2007a).

Importantly, the STN is a very small nucleus in the basal ganglia (Dormont et al., 2004). It borders and is surrounded by anatomical structures which can serve as additional landmarks to delineate the STN: (1) the substantia nigra (SN) pars compacta and pars reticularis with its caudal extension; the STN is located as a roof above the substantia nigra, (2) the red nucleus, rostral to the STN. Both the SN and red nucleus contain iron, resulting in a hypointense signal in T2 and T2*-weighted images, and high susceptibility values in susceptibility maps (Schäfer et al., in press) and are therefore easily discernable (Dormont et al., 2004). However, there is no clearly visible border between the anterior medial part of the STN and SN, and special precaution must be taken if one aims to manually segment the STN. Hence, it is vital to precisely localize the STN either on an individual level or by means of STN probability masks derived from ultra-high resolution 7 Tesla (T) magnetic resonance imaging (MRI) (Cho et al., 2010). In turn, individual or probability STN masks can be used to extract the BOLD signal in functional MRI experiments or to compute probabilistic tractography white matter tract strength between cortico-subcortical networks.

This study builds upon the methodology of previous work (Forstmann et al., 2008, 2010) that characterized the functional and structural cortico-subcortical networks which implement the flexible adjustment of response thresholds under time pressure. However, the results were inconclusive about the role of the STN in heightening response thresholds and inducing response slowing. The present study set out to investigate cortico-subthalamic white matter tract strength in stopping a motor response.

In a first step, we acquired ultra-high resolution 7T images to individually segment the STN. Next, we computed probability maps to quantify the variability in volume and location of the STN across

* Corresponding author at: University of Amsterdam, Plantage Muidergracht 24, 1018 TV Amsterdam, the Netherlands. Fax: +31 20 6390279.
*E-mail address:* b.u.forstmann@uva.nl (B.U. Forstmann).

1053-8119/$ – see front matter © 2011 Elsevier Inc. All rights reserved.
doi:10.1016/j.neuroimage.2011.12.044

subjects and to provide STN atlas templates in MNI-space. Creating probability maps of the STN using 7T MRI and applying these new maps in combination with diffusion weighted imaging (DWI) is unprecedented and STN templates are made freely available (http://www.fmrib.ox.ac.uk/fsl/data/atlas-descriptions.html). Finally, we tested whether white matter tract strength between rIFC-STN and pMFC-STN, i.e., ACC to STN and pre-SMA to STN, can be predicted by the individual efficacy to withhold a motor response, measured by the stop signal reaction time (SSRT).

## Methods

An overview of the methods used in the two experiments is displayed in a flowchart in Fig. S1 of the Supplementary Information.

### *Participants*

For the computation of the STN probability maps, thirteen participants (six females) were scanned. The participants were on average 24.38 years old (range: 22–28, standard deviation: 2.36). Only eight young participants (four females) participated in the stop-signal task for a small monetary reward of 8 euros. One subject had to be excluded because of technical problems during the behavioural session. The remaining participants were on average 24.87 years old (range: 22–28, standard deviation: 2.23). For the replication study, fourteen participants (eight females) were scanned and behaviourally tested. The participants were on average 24.29 years old (range: 18–33, standard deviation: 4.86). All participants signed a consent form before the scanning session. All participants had normal or corrected-to-normal vision, and none of them had a history of neurological, major medical, or psychiatric disorders. All subjects were right-handed, as confirmed by the Edinburgh Inventory (Oldfield, 1971). The study was approved by the local ethics committee and subjects gave their written informed consent.

### *Behavioural task*

As shown in Fig. 1, we used a stop-signal paradigm which slightly differed for the replication study (for further details, see the section Independent replication study and Jahfari et al. (2011)). Participants were instructed to respond with either the left or right index finger to an arrow pointing either to the left or right, respectively. Instructions emphasized on both speed and accuracy. However, on one third of all trials, a sound (stop-signal) appeared and participants were instructed to withhold the indicated response and not to press a button at all. The delay between the go stimulus (arrows pointing left or right) and the stop signal, i.e., the stop signal delay (SSD), was adjusted according to the staircase method separately for left and right hand responses. This ensured a convergence to P (inhibit) of 50% at the end of the experiment. For example, if a stop signal was presented and the subject responded, then the stop signal delay was reduced by 20 ms on the subsequent stop trial; if the subject did not respond (i.e., successfully stopped response), then the stop signal delay was increased by 20 ms. The SSD value for the stop sound was initially set to 250 ms for both left and right hand responses. Each trial had a fixed time length of 3000 ms. The SSRTs were estimated using the so-called 'integration method' (Logan and Cowan, 1984; Verbruggen and Logan, 2009). On go trials, participants received feedback of 500 ms if they responded too slowly (i.e., RT > 700 ms after arrow stimulus). In total 420 go-trials, and 180 stop-trials were presented. The experiment lasted for approximately 35 min.

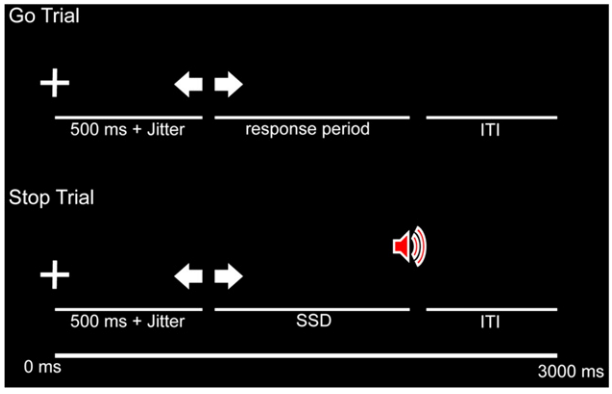


**Fig. 1.** Stop-signal paradigm.

### *Data acquisition of ultra-high resolution anatomical images*

Participants underwent structural scanning on a 7T Magnetom MRI system (Siemens, Erlangen) using a 24-channel head array Nova coil (NOVA Medical Inc., Wilmington MA, USA). Whole brain images were acquired with an MP-RAGE (Deichmann et al., 2000) sequence (TR = 3000 ms, TE = 2.95 ms, TI = 1100 ms, voxel size: 0.8 mm isotropic, flip angle = 6°, GRAPPA acceleration factor 2). Moreover, a multiecho spoiled 3 dimensional (3D) gradient echo (FLASH) (Elolf et al., 2007; Haase et al., 1986) sequence (TR = 43 ms, TE = 11.22 ms, TE = 21.41 ms, TE = 31.59 ms, flip angle = 13°, voxel $0.5 \times 0.5 \times 0.6$ mm³, 56 coronal slices) was acquired. To assess replicability of the results, the FLASH sequences were repeated during each session and for each participant. Subsequently, correlations for all voxels within each individual STN mask, which were drawn on the FLASH images, were computed within sessions. For each participant, the results showed a high correlation between voxels ($r > 0.8$). Acquisition time was approximately 60 min for each session. The T1-weighted MP-RAGE scans were co-registered into MNI152 template and the FLASH images were registered on the T1 images using rigid-body transformations with a mutual information cost function as implemented in FSL (www.fmrib.ox.ac.uk/fsl).

### *Manual segmentation of the STN*

Manual segmentation was performed using the FSL 4.1.4 viewer. Segmentation was carried out by two independent researchers and inter-rater agreement was assessed (see Supplemental Information). Only voxels rated by both raters as belonging to the STN were included in any further analysis. The manual segmentation was done as follows: In an initial step, the individual volumes obtained with the three different echoes of the FLASH sequence were loaded into the viewer. This was done separately for each participant. Second, the contrast values in the viewer for the three different images were set to maximally increase visibility of the STN. Third, the coronal view was singled out and zoomed in to facilitate the drawing of the STN mask by going back and forth between the three different echoes. Finally, inter-rater reliability (mean/SD of Cohen's kappa = 0.86/0.05) and intraclass correlation coefficients of STN volumes as a measure of agreement between the two raters ($r = 0.94$) were obtained (see Supplemental Information).

### *Computation of probability maps and atlasing of the STN*

The STN masks were delineated in the acquisition space of the T2*-weighted FLASH images, which covered a thin region oriented coronally and centred on the subthalamic region. To register these masks to MNI standard space, the masks were first aligned to the MPRAGE image of the same subject, before transferring the subject to standard space. Due to B1 inhomogeneities at 7T the registration from FLASH to MPRAGE required a semi-automated approach based on landmark correspondence. First, we identified and selected the following landmarks on the anatomy: the posterior commissure, the top

indention of the pons, the start of the trigeminal nerves out of the brainstem, left and right, and the top of the crux of the fornix. These five landmarks are reliably identifiable in both contrasts, and surround the region of the STN. Landmark identifications were performed in triplanar views displaying both images simultaneously in the MIPAV software package (http://mipav.cit.nih.gov). Second, the FLASH image was transferred into subject space with a rigid transformation estimated from the landmarks. Inaccuracies in the landmarks placement may result in some misalignment, so we refined the alignment with an automated registration step. The Optimized Automated Registration algorithm included in MIPAV is used for this step, after masking out areas of the MPRAGE not present in the FLASH image. Third, the subjects were linearly registered to the MNI152 template at 0.5 mm resolution with the same algorithm, after extracting the brain on the 7T MPRAGE image with the SPECTRE algorithm (Carass et al., 2011). The delineations of the STN were transferred through multiple transformations to MNI space. To compensate for interpolation in these small structures, the signed distance functions for each of the masks was computed first, transferred those, and obtained the final delineations by thresholding the transformed distance functions. Once the delineations were in MNI space, a statistical atlas was generated by averaging the masks. Resulting probability maps were then thresholded at zero separately for the left and right STN in MNI space. Given the small size of the STN, the multiple registration steps and the anatomical variability, the statistical atlas was checked for outliers by comparing the average probability for each delineated mask resulting in discarding one subject that fell below one standard deviation of the original atlas.

*Data acquisition and preprocessing of diffusion-weighted data*

With a 32-channel array head coil and a maximum gradient strength of 40 mT/m, diffusion-weighted data and T1 weighted images (3D MPRAGE) were acquired on a Siemens 3T Tim Trio scanner (Siemens, Erlangen). The diffusion-weighted data were acquired using spin-echo echo planar imaging (TR = 11 s, TE = 90 ms, 85 axial slices, resolution $1.5 \times 1.5 \times 1.5$ mm, GRAPPA acceleration factor = 3). Diffusion weighting was isotropically distributed along 60 directions (b-value = 1000 s/mm$^2$, AV = 3). Note that high angular resolution of the diffusion weighting directions yields robust estimation of the fiber directions by increasing the signal-to-noise ratio and reducing directional bias. Seven data sets with no diffusion weighting (b0) were acquired; one image in the beginning of the diffusion scanning sequence and one image after each block of ten diffusion-weighted images. These images served as an anatomical reference for offline motion correction. The acquisition of this protocol lasted approximately 42 min.

All baseline b0 images were aligned to a reference b0 image to estimate motion correction parameters using rigid-body transformations implemented in FLIRT (Jenkinson and Smith, 2001). The resulting linear transformation matrices were combined with a global registration to the T1 anatomy computed with the same method. The gradient direction for each volume was corrected using the rotation parameters. The transformation matrices were applied to the diffusion-weighted images, and the three corresponding acquisitions and gradient directions were averaged to improve signal-to-noise ratio (Behrens et al., 2007).

*Tractography*

Diffusion image preprocessing and analyses were done using FSL 4.1.4 (www.fmrib.ox.ac.uk/fsl). In accordance with Behrens et al. (2003), estimation of tracts was conducted using probabilistic tractography. A probabilistic fiber tracking approach was chosen, using 5000 tract-following samples at each voxel with a curvature threshold of 0.2. A dual-fiber model as implemented in the latest version of bedpostX (FSL 4.1.4) was used. Dual-fiber models account for crossing fibers (Behrens et al., 2007) therefore yielding more reliable results compared to single-fiber models. All tractography was done in each participant's native space (un-normalized) data, and resulting maps were warped into standard space (using the MNI 1 mm isotropic brain as reference) for cross-participant averaging and comparison. For the estimation of tract strength between cortex and left and right STN, respectively, MNI-space cortical masks were normalized to each participant's native space, using the inverse of the normalization parameters. Visual inspection ensured that tractography maps were successful and acceptable for further analysis. Individually segmented ultra-high resolution left and right STN masks were used (see also Manual segmentation of the STN).

Seed-based classification was done by first thresholding the images such that only voxels with at least ten samples are kept (Aron and Poldrack, 2006; Aron et al., 2007). Next, voxel values were converted into proportions, i.e. white matter tract strength, such that the value at each voxel becomes the number of samples reaching the target mask for that image, divided by the number of samples from the seed mask. Seed-based classification was done from the left and right IFC, the left and right ACC, and the left and right pre-SMA, into the left and right STN, respectively (Fig. 2). Since directionality cannot be inferred from tractography analyses, seed-based classification was also done from the left and right STN to the left and right pre-SMA, the left and right ACC, and the left and right IFC, respectively. Again proportions were computed. The proportion values resulting from cortical seed masks to STN and proportion values resulting from STN seed masks to cortex were averaged, e.g. the proportion value from left pre-SMA to left STN and the proportion value from left STN to left pre-SMA. Note that a contralateral exclusion mask was used to circumvent that, e.g., fibers from the left pre-SMA would first project to the right pre-SMA and then project to the left or right STN. The averaged proportion values were later used for correlations with the individual SSRT measure. All analyses were done separately for each hemisphere.

*Independent replication study*

In the second study, i.e. the replication study, a combination of the Simon task (Simon, 1967) and the stop-signal task (Logan and Cowan,

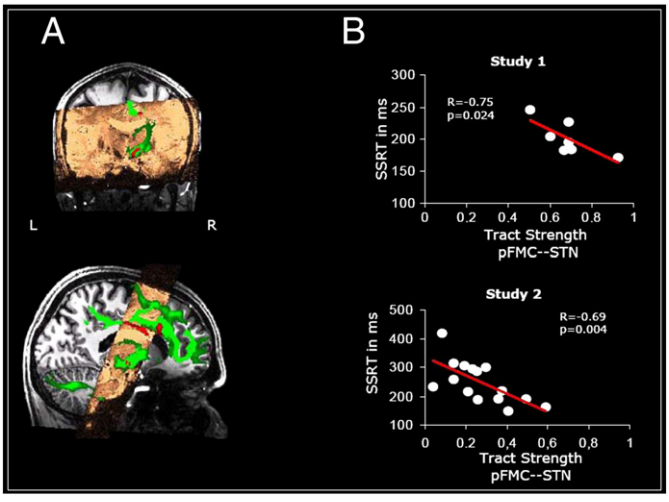


**Fig. 2.** Tract strength between pMFC and STN is predicted by increased individual efficacy to withhold a motor response. A) Connectivity-based seed classification for the right ACC (red) projecting into the right STN (red) rendered on the ultra-high resolution 7 T MRI scans (copper) and the white matter tract connecting between the right ACC and the right STN (green). B) Individual differences in tract strength between the right ACC and the right STN are associated with more efficient stopping of a motor response. Lower right panel shows results of an independent replication study using the STN probability maps as seed masks. (For interpretation of the references to colour in this figure legend, the reader is referred to the web of this article.)

1984) with four different target colours was used (see also Jahfari et al. (2011)). On go trials, participants were instructed to press a left response button (with the left index finger) if a yellow or blue square was presented and to press a right response button (with the right index finger) if a red or green square was presented. The colour mapping (e.g., blue/yellow, press left) was counterbalanced across subjects. A trial started with the presentation of a fixation cross, followed by a coloured square that could appear on the left or right side of the screen. On corresponding trials (C), responses were spatially compatible with the position of the target (e.g., blue square on the left side of the screen indicating a left hand button press), whereas on non-corresponding trials (NC), responses were opposite with respect to the target location (e.g., blue square on the right side of the screen indicating a left hand button press). Instructions emphasized that participants should try to respond as fast as possible to the colour of the presented stimuli while ignoring the location. In addition, participants were instructed to stop the indicated response if the go stimulus was followed by a sound (stop-signal). The SSD between the go stimulus (the coloured square) and the stop signal was dynamically adjusted separately for C and NC trials according to the staircase method to ensure convergence to P (inhibit) of 0.5. For example, if a stop signal was presented on a C trial and the subject responded (Failed Stop), then the SSD for the C staircase was reduced by 50 ms on the subsequent C stop trial; if the subject did not respond (i.e., Successful Stop), then SSD was increased by 50 ms. Initial SSD set to 250 ms for both C and NC stop trials. Each trial had a fixed time length of 4000 ms. If participants had not responded within a time window of 1250 ms after go stimulus presentation, feedback stating 'te langzaam' ('too slow', in Dutch) for a duration of 2000 ms was presented. Participants performed two experimental blocks with a total of 192 go trials (96 corresponding; 96 non-corresponding), and 64 stop trials (32 corresponding; 32 noncorresponding). As before, SSRTs were estimated for each individual subject (see Jahfari et al. (2011) for further details).

The fourteen participants also underwent two runs of diffusion-weighted scans on a 3T scanner (Philips Medical Systems, Best, The Netherlands). Subsequently, the two DWI scans were pooled for further analysis. Note that this data has not been reported previously. Probabilistic tractography was computed using the same cortical and subcortical masks as in the first study presented above. Importantly, in this study, the probability STN maps were used as seed and target masks for the tractography analyses.

## Results

### *Behavioural results*

Behavioural results of the first study are displayed in Table 1. In both studies there were no main effects between response hands for Go reaction times, SSRTs or SSDs. In the second study, no significant differences were found between C and NC trials (see also Jahfari et al. (2011)).

**Table 1**
Mean stop-signal reaction times (SSRT) and mean Go reaction times (RT) of the first study.

| | All | Left | Right |
|---|---|---|---|
| Go | | | |
| Mean RT (ms) | 497.42 (108.49) | 498.33 (112.70) | 496.46 (105.70) |
| Errors (%) | 0.35 (0.58) | 0.42 (0.82) | 0.30 (0.44) |
| Stop respond | | | |
| Mean RT (ms) | 454.89 (96.23) | 453.08 (104.22 | 457.21 (88.38) |
| Stop inhibit | | | |
| SSD (ms) | 293.92 (139.90) | 291.58 (126.81) | 296.28 (139.25) |
| P inhibit (%) | 0.50 (0.01) | 0.50 (0.01) | 0.51 (0.02) |
| SSRT (ms) | 196.21 (28.18) | 197.97 (30.14) | 195.37 (35.52) |

SSD = Stop-signal delay; P inhibit = probability to inhibit; ms = milliseconds.

### *Cortico-subthalamic networks and stopping a motor response*

The results of the first study of our diffusion weighted structural analyses are depicted in Fig. 2 upper right panel. Our data show that interindividual differences in the efficacy to stop a motor response as reflected by short SSRTs predicted increased structural connections between the ACC and right STN ($R = -0.75$, $p = 0.024$, uncorrected), whereas no such association was present for the connections between other considered brain areas, including the connections from rIFC to either the left or right STN, respectively.

The results of the second replication study confirmed that tract strength between the ACC and the STN was predicted by the individual efficacy with which participants withheld a motor response ($R = -0.69$, $p = 0.004$, corrected) (Fig. 2 lower right panel). Note that this replication study and its analyses are statistically independent from the first study (for an overview see Fig. S1); hence, the probability that the measured strength of the same tract as before would once again yield the highest correlation with SSRTs is small (i.e., 1/12, because twelve connections were tested) and the probability that this correlation would again be significant is very small (<0.0037).

### *Atlasing of the subthalamic nucleus*

Fig. 3 shows STN probability maps derived from thirteen participants. The highest overlap across participants for the left STN was 45.83% (peak MNI coordinate: $x = -8$, $y = -13.5$, $z = -7$). For the right STN, the highest overlap across participants was 50% (peak MNI coordinate: $x = 11$, $y = -12.5$, $z = -7$). The volume of the left and the right probabilistic STN mask was 692.25 $mm^3$ and 687.25 $mm^3$, respectively. Note that the volumes of the probability maps overestimate the volumes of individuals STN masks. Table 2 depicts each individuals left and right STN volume; the individual STN masks were used to generate the probability maps. The mean volume of the left and right individuals STN was 61.69 $mm^3$ and 50.47 $mm^3$, respectively.

## Discussion

In a previous study, we provided functional and structural evidence for the pre-SMA in concert with the striatum to implement the flexible adjustment of response thresholds under time pressure (Forstmann et al., 2008, 2010). However, the results were inconclusive about the role of the STN in heightening response thresholds and therefore inducing response slowing. The present study set out to investigate cortico-subthalamic white matter tract strength in stopping a motor response.

In the present study, ultra-high resolution 7T data was acquired to segment the STN individually and to provide probability maps of the STN in MNI-space (Fig. 3). As can be seen from the probability maps and individuals' STN masks (Table 2), both volume and precise localization of the STN reveal interindividual variability in young healthy subjects. Moreover, recent papers often make use of a $10 \times 10 \times 10$ mm box mask (see, e.g., Neubert et al. (2010)) centred around the MNI-peak coordinate (10, −15, −5) provided by Aron and colleagues (Aron and Poldrack, 2006; Aron et al., 2007). However, given the extent of this anatomical ROI, it is evident that also parts of the SN fall into this mask. This limitation can now be overcome by using the present probability maps which will be made freely available (http://www.fmrib.ox.ac.uk/fsl/data/atlas-descriptions.html).

The results of our diffusion weighted structural analyses are depicted in Fig. 2. Our data show that participants who are very efficient in stopping a motor response, as reflected by short SSRTs, have stronger structural connections between the ACC and right STN whereas no such association was present for the connections between other considered brain areas, including the connections from rIFC to either the left or right STN, respectively. To test the specificity of these results using STN probability maps, a second independent replication study was conducted. Fig. 2B (lower panel) shows that a

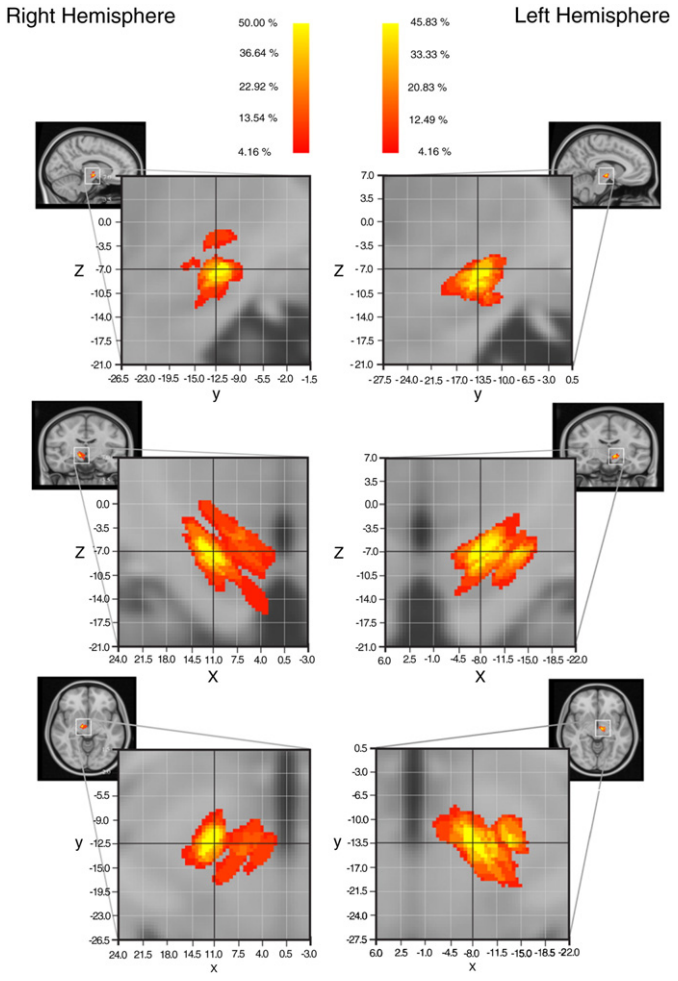


**Fig. 3.** Probability maps are based on thirteen individually segmented left and right 7T MRI STN masks. Peak overlap MNI coordinate for the left STN ($x=-8$, $y=-13.5$, $z=-7$); peak overlap MNI coordinate for the right STN ($x=11$, $y=-12.5$, $z=-7$). The colour bar indicates the overlap of subjects in percentage. The volume of the left probabilistic STN mask is 692.25 $mm^3$. The volume of the right probabilistic STN mask is 687.25 $mm^3$.

comparable negative correlation is found with an increase in tract strength between the ACC and the left STN and faster SSRTs. Note that the tract strength measures were lower in the second study compared to first study. One explanation is the use of the probability maps instead of ultra-high resolution 7T individual STN masks yielding a lower signal to noise ratio in the DWI tract strength analyses. Even though we argue that these new probability maps are anatomically more precise than previous approaches reported in the literature, we acknowledge the substantial interindividual variability in STN volume (Table 2). Another explanation could be the differences in DWI scan acquisition parameters between the first and the second study. Importantly, in the second study there was again no correlation found for the tract strength between the rIFC and the STN with individual differences in SSRTs.

**Table 2**
Individual volume estimates for the left and right STN for the thirteen participants of the first study using ultra-high resolution 7T MRI.

| Subjects | Left STN ($mm^3$) | Right STN ($mm^3$) |
|---|---|---|
| pp01 | 79.80 | 56.85 |
| pp02 | 49.80 | 33.30 |
| pp03 | 31.74 | 71.61 |
| pp04 | 84.60 | 40.65 |
| pp05 | 44.10 | 20.70 |
| pp05 | 42.30 | 31.35 |
| pp07 | 109.35 | 80.10 |
| pp08 | 43.65 | 34.35 |
| pp09 | 52.65 | 43.20 |
| pp10 | 59.70 | 49.50 |
| pp11 | 96.00 | 73.95 |
| pp12 | 36.00 | 49.05 |
| pp13 | 72.30 | 71.55 |
| *Mean (stdev)* | 61.69 (24.51) | 50.47 (18.97) |

In sum, our results are in line with the pMFC-subthalamic theory to implement efficient response inhibition in a stop-signal task. This finding is corroborated by neurocomputational models arguing for a central role of the ACC in, e.g., the detection of conflict yielding a slowing of motor responses (Botvinick et al., 2001). In the present study, we suggest that the ACC might signal the need to implement a change of motor behaviour by breaking or stopping the response which is accomplished by an excitatory signal to the STN (Neubert et al., 2010). Hence, participants with higher tract strength within this cortico-subthalamic network are more efficient to withhold a motor response. This relation was not present for the rIFC-STN connection which is in line with a recent study by Aron and colleagues (Aron and Poldrack, 2006; Aron et al., 2007). However, the exact role of the rIFC in response inhibition needs to be determined. Recent TMS studies indicated that the rIFC has an inhibitory effect on M1 when participants have to cancel an initiated action (Buch et al., 2010), and that the ventral part of this region might play an important role in the updating of action plans (Verbruggen et al., 2010). At the same time, other studies have pointed out that rIFC might have a pure attentional role (Sharp et al., 2010), while the medial frontal cortex resolves the conflict between the go and stop signal.

In conclusion, findings from the present study provide evidence for the interindividual variability of the STN which renders the precise localization of this small basal ganglia nucleus necessary. Functionally, the results indicate that the ACC-subthalamic pathway plays a crucial role in the process of response inhibition. Individual variability in withholding a motor response predicted the connection strength between cortex and STN pointing to a top-down controlled inhibitory network that is intricately linked to behavioural performance.

## Acknowledgments

This work was supported by VENI (BUF) and Mozaiek grant (SJ) from the Netherlands Organization for Scientific Research (NWO) and by the Federal Ministry of Education and Research, Germany, FKZ:01EO1001 (JN).

## Appendix A. Supplementary data

Supplementary data to this article can be found online at doi:10.1016/j.neuroimage.2011.12.044.

## References

Aron, A.R., Poldrack, R.A., 2006. Cortical and subcortical contributions to Stop signal response inhibition: role of the subthalamic nucleus. J. Neurosci. 26 (9), 2424–2433.
Aron, A.R., Behrens, T.E., Smith, S., Frank, M.J., Poldrack, R.A., 2007. Triangulating a cognitive control network using diffusion-weighted magnetic resonance imaging (MRI) and functional MRI. J. Neurosci. 27 (14), 3743–3752.
Behrens, T.E., Johansen-Berg, H., Woolrich, M.W., Smith, S.M., Wheeler-Kingshott, C.A., Boulby, P.A., et al., 2003. Non-invasive mapping of connections between human thalamus and cortex using diffusion imaging. Nat. Neurosci. 6 (7), 750–757.
Behrens, T.E., Berg, H.J., Jbabdi, S., Rushworth, M.F.S., Woolrich, M.W., 2007. Probabilistic diffusion tractography with multiple fibre orientations: what can we gain? NeuroImage 34 (1), 144–155.
Bogacz, R., Wagenmakers, E.J., Forstmann, B.U., Nieuwenhuis, S., 2010. The neural basis of the speed–accuracy tradeoff. Trends Neurosci. 33 (1), 10–16.
Botvinick, M.M., Braver, T.S., Barch, D.M., Carter, C.S., Cohen, J.D., 2001. Conflict monitoring and cognitive control. Psychol. Rev. 108 (3), 624–652.

Buch, E.R., Mars, R.B., Boorman, E.D., Rushworth, M.F.S., 2010. A network centered on ventral premotor cortex exerts both facilitatory and inhibitory control over primary motor cortex during action reprogramming. J. Neurosci. 30 (4), 1395–1401.
Carass, A., Cuzzocreo, J., Wheeler, M.B., Bazin, P.-L., Resnick, A.S., Prince, J.L., 2011. Simple paradigm for extra-cerebral tissue removal: algorithm and analysis. NeuroImage 56, 1982–1992.
Cho, Z.H., Min, H.K., Oh, S.H., Han, J.Y., Park, C.W., Chi, J.G., et al., 2010. Direct visualization of deep brain stimulation targets in Parkinson disease with the use of 7-Tesla magnetic resonance imaging. J. Neurosurg. 113 (3), 639–647.
Deichmann, R., Good, C.D., Josephs, O., Ashburner, J., Turner, R., 2000. Optimization of 3-D MP-RAGE sequences for structural brain imaging. NeuroImage 12 (1), 112–127.
Dormont, D., Ricciardi, K.G., Tande, D., Parain, K., Menuel, C., Galanaud, D., et al., 2004. Is the subthalamic nucleus hypointense on T2-weighted images? A correlation study using MR imaging and stereotactic atlas data. AJNR Am. J. Neuroradiol. 25 (9), 1516–1523.
Elolf, E., Bockermann, V., Gringel, T., Knauth, M., Dechent, P., Helms, G., 2007. Improved visibility of the subthalamic nucleus on high-resolution stereotactic MR imaging by added susceptibility (T2*) contrast using multiple gradient echoes. AJNR Am. J. Neuroradiol. 28 (6), 1093–1094.
Forstmann, B.U., Dutilh, G., Brown, S., Neumann, J., von Cramon, D.Y., Ridderinkhof, K.R., et al., 2008. Striatum and pre-SMA facilitate decision-making under time pressure. Proc. Natl. Acad. Sci. U. S. A. 105 (45), 17538–17542.
Forstmann, B.U., Anwander, A., Schafer, A., Neumann, J., Brown, S., Wagenmakers, E.J., et al., 2010. Cortico-striatal connections predict control over speed and accuracy in perceptual decision making. Proc. Natl. Acad. Sci. U. S. A. 107 (36), 15916–15920.
Frank, M.J., Samanta, J., Moustafa, A.A., Sherman, S.J., 2007a. Hold your horses: impulsivity, deep brain stimulation, and medication in parkinsonism. Science 318 (5854), 1309–1312.
Frank, M.J., Scheres, A., Sherman, S.J., 2007b. Understanding decision-making deficits in neurological conditions: insights from models of natural action selection. Philos. Trans. R. Soc. Lond. B Biol. Sci. 362 (1485), 1641–1654.
Haase, A., Frahm, J., Matthaei, D., Hanicke, W., Merboldt, K.D., 1986. FLASH imaging: rapid NMR imaging using low flip angle pulses. J. Magn. Reson. 67, 258–266.
Jahfari, S., Waldorp, L., van den Wildenberg, W.P., Scholte, H.S., Ridderinkhof, K.R., Forstmann, B.U., 2011. Effective connectivity reveals important roles for both the hyperdirect (fronto-subthalamic) and the indirect (fronto-striatal-pallidal) fronto-basal ganglia pathways during response inhibition. J. Neurosci. 31 (18), 6891–6899.
Jenkinson, M., Smith, S.M., 2001. A global optimisation method for robust affine registration of brain images. Med. Image Anal. 5, 143–156.
Logan, G., Cowan, W., 1984. On the ability to inhibit throught and action: a theory of an act of control. Psychol. Rev. 91 (3), 295–327.
Mink, J., 1996. The basal ganglia: focused selection and inhibition of competing motor programs. Prog. Neurobiol. 50, 381–425.
Nambu, A., Tokuno, H., Takada, M., 2002. Functional significance of the cortico-subthalamo-pallidal 'hyperdirect' pathway. Neurosci. Res. 43 (2), 111–117.
Neubert, F.X., Mars, R.B., Buch, E.R., Olivier, E., Rushworth, M.F.S., 2010. Cortical and subcortical interactions during action reprogramming and their related white matter pathways. Proc. Natl. Acad. Sci. U. S. A. 107 (30), 13240–13245.
Oldfield, R.C., 1971. The assessment and analysis of handedness: the Edinburgh inventory. Neuropsychologia 9 (1), 97–113.
Schäfer, A., Forstmann, B.U., Neumann, J., Wharton, S., Mietke, A., Bowtell, R., Turner, R., in press. Direct visualization of the subthalamic nucleus and its iron distribution using high-resolution susceptibility mapping. Hum. Brain Mapp. doi:10.1002/hbm.21404 (Electronic publication ahead of print).
Sharp, D.J., Bonnelle, V., De Boissezon, X., Beckmann, C.F., James, S.G., Patel, M.C., et al., 2010. Distinct frontal systems for response inhibition, attentional capture, and error processing. Proc. Natl. Acad. Sci. 107 (13), 6106–6111.
Simon, J.R., 1967. Ear preference in a simple reaction-time task. J. Exp. Psychol. 75 (1), 49–55.
Verbruggen, F., Logan, G.D., 2009. Models of response inhibition in the stop-signal and stop-change paradigms. Neurosci. Biobehav. Rev. 33 (5), 647–661.
Verbruggen, F., Aron, A.R., Stevens, M.A., Chambers, C.D., 2010. Theta burst stimulation dissociates attention and action updating in human inferior frontal cortex. Proc. Natl. Acad. Sci. U. S. A. 107 (31), 13966–13971.